Microstructural origin of soft magnetic properties of sendust films prepared by N_2 reactive sputtering

Yingjian Chen[a]
Data Storage Systems Center, Carnegie Mellon University, Pittsburgh, Pennsylvania 15213

Patrick J. Ryan and James F. Dolejsi
Seagate Technology, 7801 Computer Avenue, Bloomington, Minnesota 55435

Maithri Rao, David E. Laughlin, and Mark H. Kryder
Data Storage Systems Center, Carnegie Mellon University, Pittsburgh, Pennsylvania 15213

Ghanim Al-Jumaily and Zhijun Yang
Seagate Technology, 7801 Computer Avenue, Bloomington, Minnesota 55435

(Received 2 September 1997; accepted for publication 20 April 1998)

Sendust films were deposited using dc magnetron sputtering at room temperature in a mixture of Ar and N_2 gas. The soft magnetic properties of the sendust films were, in general, improved with the addition of N_2. The optimum soft magnetic properties were achieved when 6% N_2 gas was used. Transmission electron microscopy studies showed that the sendust film without N_2 contains average grain sizes of 200 nm; whereas the films with increasing N_2 content contain increasing percentages of much smaller grains of 20 nm. The smaller grains have a random crystalline orientation with respect to each other. The cross-sectional morphological structures were studied using a scanning electron microscope. In the film without N_2, power-law cone structures were observed. In the N_2 containing films, needlelike morphological structures were formed. X-ray photoelectron spectroscopy studies on these films indicate that N_2 included in the films reacts preferentially with Al to form AlN. Excess N_2 may then react with Si, possibly to form Si_3N_4. The atomic concentrations of Al and N become equal in the films when 6% N_2 was used, which also gives rise to the optimum soft magnetic properties. To understand the advent of soft magnetic properties, a random magnetic anisotropy model and a static wall coercive force model were considered. © *1998 American Institute of Physics.* [S0021-8979(98)06614-6]

I. INTRODUCTION

A sendust alloy consisting of about 85 wt % Fe, 10 wt % Si, and 5 wt % Al is a well known soft magnetic material. Usually soft magnetic properties in sendust alloy films are established through either a postdeposition annealing at temperatures around 400–600 °C,[1,2] or an *in situ* annealing during deposition at temperatures of about 300–400 °C.[3] It has been proposed that proper annealing transforms the disordered α-type structure in as-deposited films into an ordered DO_3-type structure.[3]

Forming the ordered DO_3 structure may not be the only way to achieve excellent soft magnetic properties. It has been reported that, by using N_2 reactive sputtering of the sendust followed by vacuum annealing at 550 °C, the morphology of the films differs from those sputtered without N_2.[8] Such a morphological change was also accompanied by an increase in permeability and electrical resistivity. The change in morphology indicates that a microstructural change may have also occurred in the N_2 containing films and may have also resulted in the changes in their magnetic properties and electrical resistivity. However, the advent of soft magnetic properties in sendust alloys without high temperature annealing is not a widely known phenomenon, and even less has been discussed about its microstructural origin.

Selective nitriding of Al in sendust films deposited in the presence of N_2 in the sputtering gas was discussed previously by Hayashi *et al.*[9] However, in the range of N_2 concentration in the films they studied, no evidence of nitriding of Si was found, and the origin of the microstructural changes as a result of N_2 inclusion was not discussed. In this study, the effects of N_2 on the microstructural, optical and magnetic properties of sendust films, particularly in their as-deposited state, are investigated. The origins of the soft magnetic properties were characterized by carrying out chemical analysis, microstructural, and morphological studies on the sendust films.

II. EXPERIMENT

Sendust films were prepared using dc magnetron sputtering at room temperature in a CVC Cluster Tool sputtering machine. The sputtering gas was a mixture of Ar and N_2. By controlling the flow rate, the percentage of N_2 in the sputtering gas was varied from 0% to 10%. Other sputtering parameters were optimized and were fixed so that N_2% was the only variable in the sputtering process. The sputtering rate was about 2.8 nm/s. All films were 3 μm thick and were deposited on AlTiC substrates.

[a]Electronic mail: yingjian.chen@readrite.com

 © 1998 American Institute of Physics

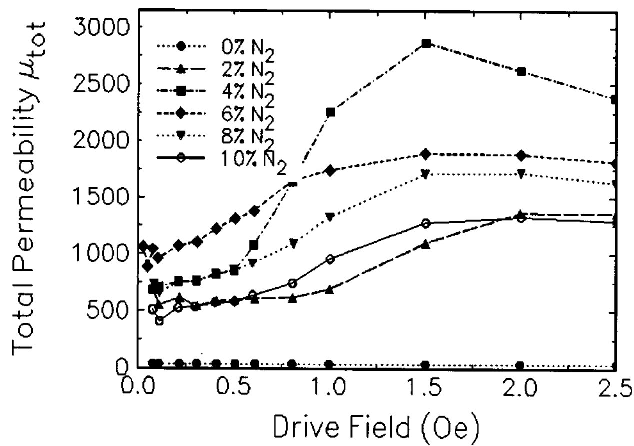

FIG. 1. Total permeabilities at varied driving fields measured using a special BH looper routine. Initial permeabilities are determined by extrapolating to zero drive field.

Magnetic properties of the films were studied using a BH hysteresis loop tracer, which has a maximum drive field of 75 Oe. A vibrating sample magnetometer was used when higher fields were needed.

Initial permeability has to be measured in zero driving field, or at least in a field much smaller than the coercivity H_c. However, signals from the BH looper would become increasingly subject to noise at such small driving fields. In our measurement, the total permeability μ_{tot}, which is the slope of the line connecting the origin and each point on the initial magnetization curve, was measured at various driving fields. The initial permeability μ_i was then determined by extrapolating μ_{tot} to zero driving field.[10]

The microstructure and crystal structures of the films were characterized using x-ray diffraction and transmission electron microscopy (TEM). Scanning electron microscopy (SEM) was used to study the morphological structure of the surface of fractured films. An atomic force microscope (AFM) was used to determine the surface roughness of the films. The electrical resistivity was measured on a Prometrix automatic resistivity tester, with a four-point probe. The refraction index n, the extinction coefficient k, the reflectance R, and the optical roughness of the films were measured using an ellipsometer.

X-ray photoelectron spectroscopy (XPS) was used to investigate the atomic concentrations of elements as well as their chemical bonding. XPS measurement involves the energy analysis of photoelectrons that are emitted from a solid as a result of monoenergetic soft x-ray excitation. In this measurement, a monochromatic Al $K\alpha$ x-ray beam (1486.6 eV) was utilized. The emitted electrons have kinetic energies given by: $E_{\text{KE}}=h\gamma-E_b-\phi$, where $h\gamma$ is the energy of the incident x-ray beam; E_b, the binding energy of the atomic orbital from which the emitted electron originates, which is used to identify the chemical species, and ϕ is the work function of the spectrometer.[11]

The samples were analyzed by depth profiling within an area having a diameter of 1 mm and up to a depth of 16 nm. The analyzed area was located approximately in the center of a sputtering crater obtained by rastering the 4 keV Ar^+ beam over an area of 3×4 mm^2. The sputter rate was approximately 2 nm/min. The energy spectra corresponding to each element were acquired and curve fitted. Chemically bonded elements were evidenced as the binding energies and were shifted from their pure unbonded states.

TABLE I. Coercivities and initial permeabilities.

	Easy axis			Hard axis			
N_2%	$4\pi M_s$ (G)	S_q	H_c (Oe)	$4\pi M_s$ (G)	S_q	H_c (Oe)	μ_i
0%	6995	0.39	50	6995	0.39	50	32
2%	8889	0.82	1.58	8860	0.56	1.78	556
4%	9327	0.93	0.77	9357	0.54	1.05	691
6%	9006	0.83	0.76	9006	0.32	0.91	1038
8%	8743	0.54	0.88	8041	0.36	1.1	728
10%	8275	0.46	1.13	8304	0.4	1.3	505

III. RESULTS

The total permeabilities of the N_2 containing films are shown in Fig. 1. The extrapolated initial permeabilities are listed in Table I.

The results from the magnetic properties measurements as listed in Table I showed that introducing N_2 up to 6% in the gas dramatically reduced coercivity and increased the initial permeability of the films. Further additions of N_2 had an adverse affect on the magnetic properties as shown in Fig. 2. With the addition of 6% N_2, the hard axis coercivity is below 1 Oe and initial permeability is over 1000. Such values are comparable to those in the films prepared with high substrate heating,[3] but not as good as those reported for the rapid thermal annealed films.[1] Saturation magnetization M_s and squareness S_q of the films were observed to increase slightly up to 4% of N_2 before they decreased at higher N_2 concentration. The films deposited in 2%–10% N_2 gas showed some weak intrinsic anisotropy. The film without N_2 has a much higher H_c value of 50 Oe, and a high magnetic field is required to reach saturation. A VSM was therefore used instead of a BH looper to measure the hysteresis loop of this film with a maximum field of 300 Oe.

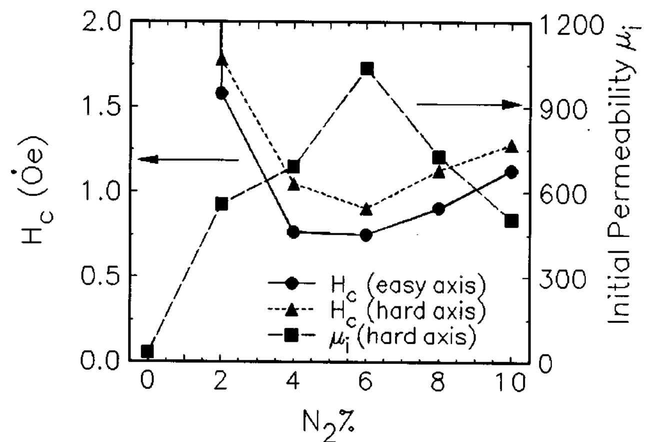

FIG. 2. Dependence of easy and hard axis coercivity and initial permeability on N_2% in the sputtering gas.

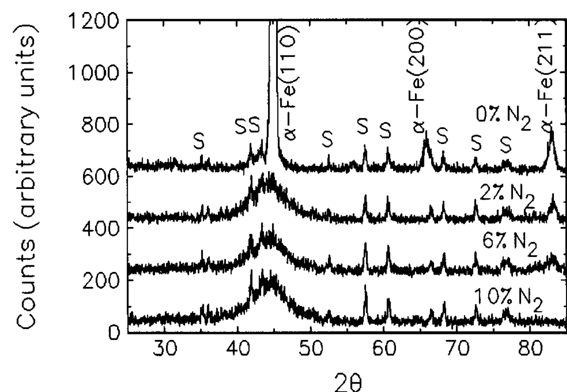

FIG. 3. X-ray diffraction of films with different N_2% in the sputtering gas (S: substrate).

X-ray diffraction patterns of the films deposited with 0%, 2%, 6%, and 10% N_2 gas are shown in Fig. 3. The N_2 additions seem to have little effect on the peak positions. The diffraction peak intensities and the peak width (FWHM) are listed in Table II. The sendust film with no N_2 additions showed a large and narrow peak corresponding to the (110) planes in the bcc structure of the sendust. Two lower intensity peaks corresponding to the (200) and (211) planes can also be observed. The (110) and (211) peaks became much lower and broader as N_2 was introduced into the films. The broadening of the α-Fe (110) and (211) peaks caused by adding N_2 to the sputtering gas indicated that a much finer grain size was achieved. The (211) peak was absent in the films deposited in 10% N_2 gas. The (200) peak was indistinguishable from the AlTiC background peak in all the N_2 containing films. No peaks associated with the iron nitrides, such as Fe_4N or $Fe_{16}N_2$ were observed.

TABLE II. X-ray diffraction peak intensities and peak width.

	Peak counts			FWHM		
N_2%	(110)	(211)	(200)	(110)	(211)	(200)
0%	3050	150	140	0.57°	0.9°	1°
2%	180	110	⋯	4.9°	0.9°	⋯
6%	160	70	⋯	5°	1.4°	⋯
10%	180	⋯	⋯	5.5°	⋯	⋯

TEM bright-field micrographs of the sendust films deposited in 0%–10% N_2 are shown in Figs. 4(a)–4(d). The film deposited without N_2 showed grains of average size of 200 nm. The electron diffraction pattern of this film is shown in Fig. 5(a). The indexed diffraction rings of this film indi-

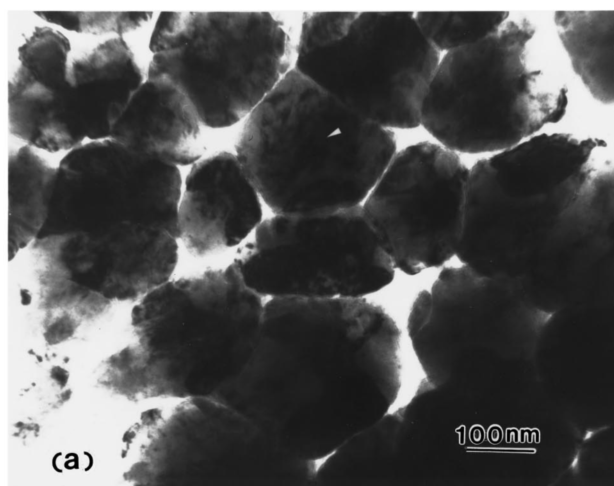

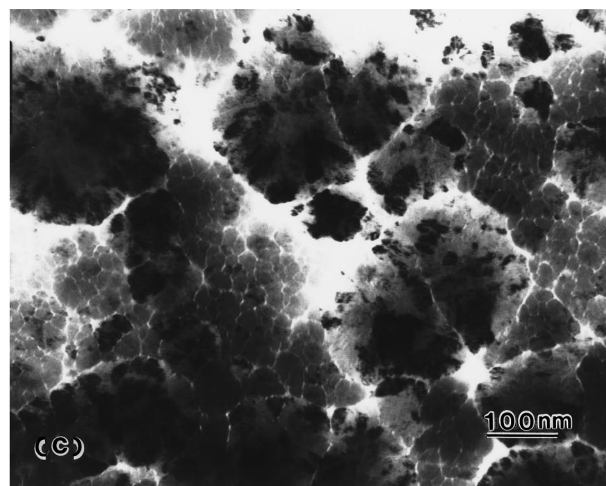

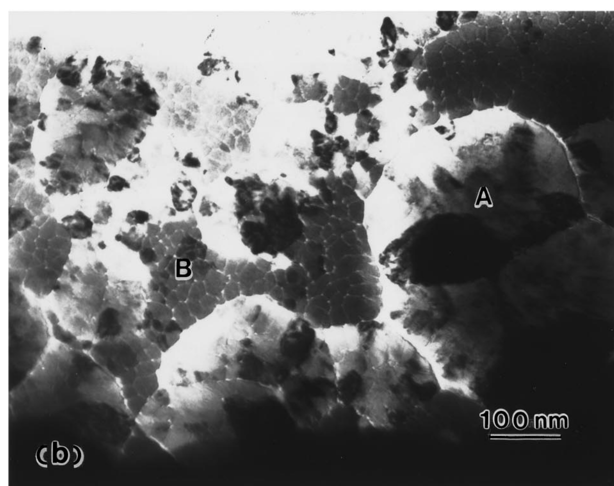

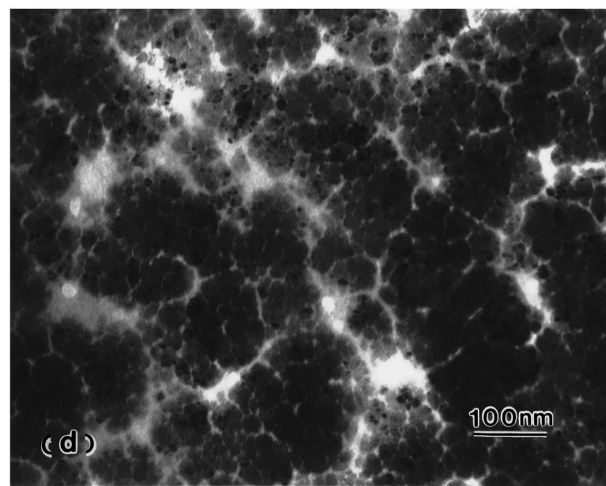

FIG. 4. (a)–(d) TEM bright-field images of sendust films deposited with (a) 0%, (b) 2%, (c) 6%, and (d) 10% N_2.

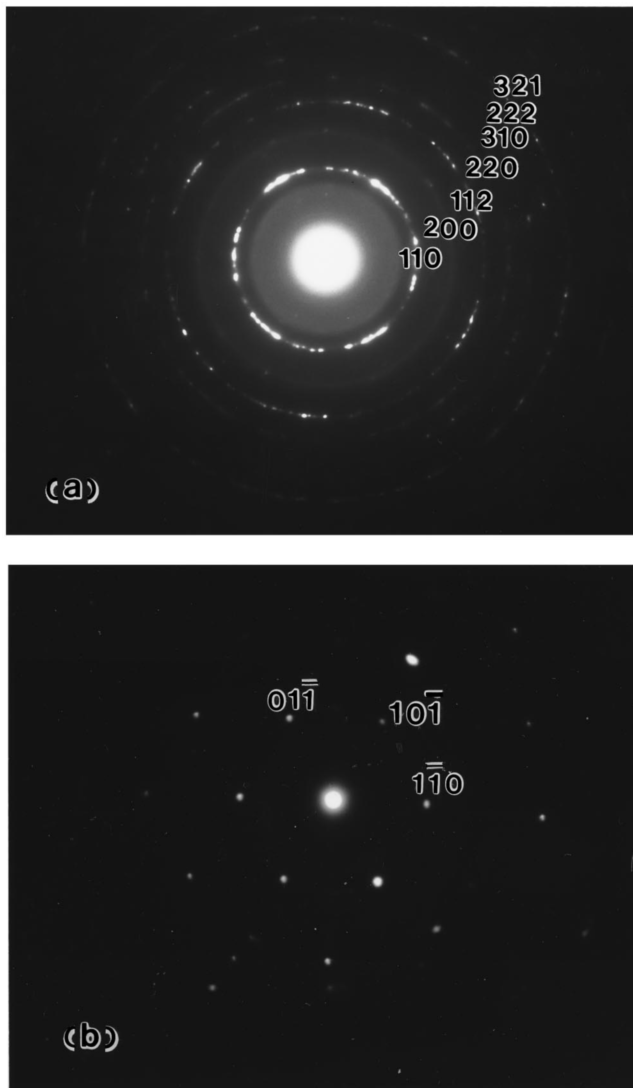

FIG. 5. Electron diffraction patterns of the sendust film with 0% N_2 (a) from an area of diameter of about 1 μm, and (b) from a single grain obtained by using selected area aperture (SAD) orientation near ⟨111⟩.

cates a nearly random crystal orientation and are consistent with the cubic bcc structure. Superlattice rings are not observed. The grains are sufficiently large that individual reflections are seen in the rings. By using a selected area diffraction (SAD) aperture, the area used for obtaining the diffraction patterns can be reduced from 1 μm to about 150–200 nm in diameter. The spot SAD pattern as shown in Fig. 5(b) was taken from one grain in the film without N_2. The grain was thus shown to be a single crystal. The film deposited with 2% N_2 contains different types of grains as shown in Fig. 4(b). There are grains of similar size to those seen in the film without N_2, and some large grains contain a varying number of grain boundaries. There are also small grains of average size 20 nm in between the larger grains. These small grains are separated by distinctive grain boundaries. The electron diffraction pattern taken with a large SAD aperture (1 μm) from the film deposited in 2% N_2 is shown in Fig. 6(a). The same but broader diffuse rings were found as compared to the film without N_2. The diffraction pattern from within a single large grain labeled A in Fig. 4(b) is shown in

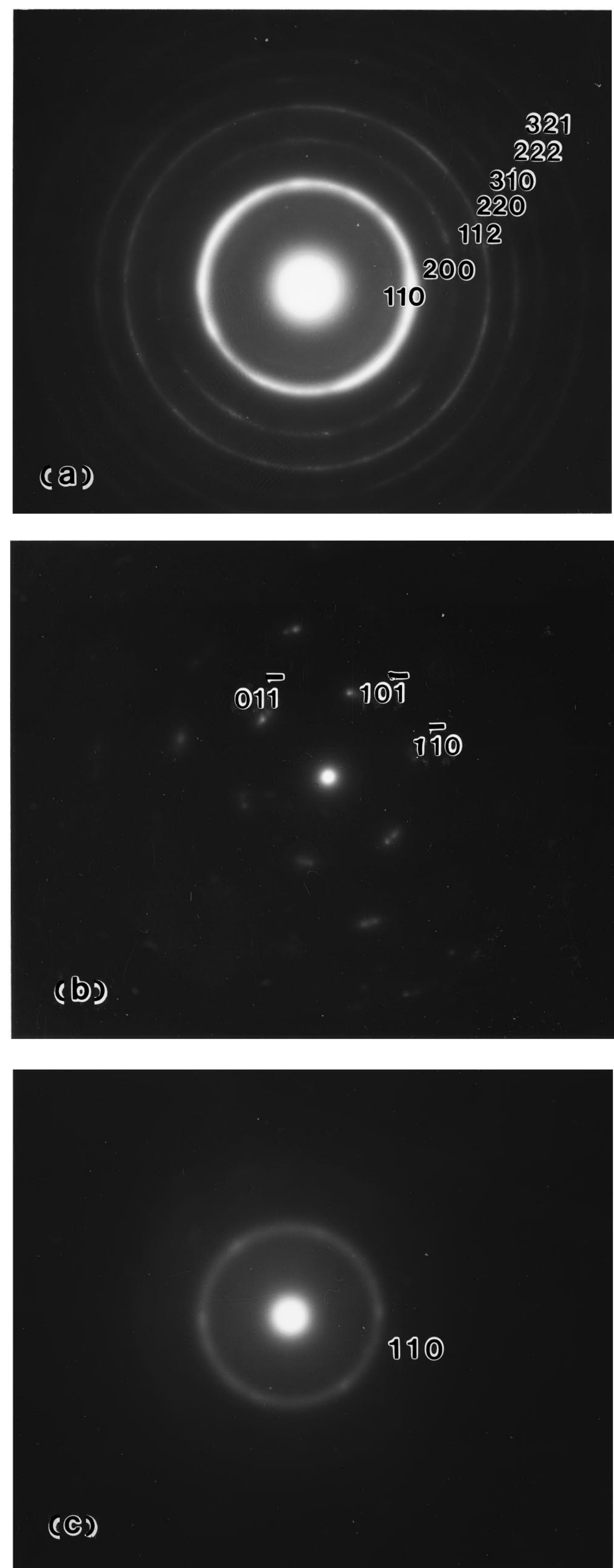

FIG. 6. Electron diffraction pattern of a sendust film deposited with 2% N_2, (a) using an electron beam of diameter of about 1 μm, (b) from a large grain of size 200 nm labeled A in Fig. 6 (b), (c) from an area containing many small 20 nm grains labeled B in Fig. 6 (b).

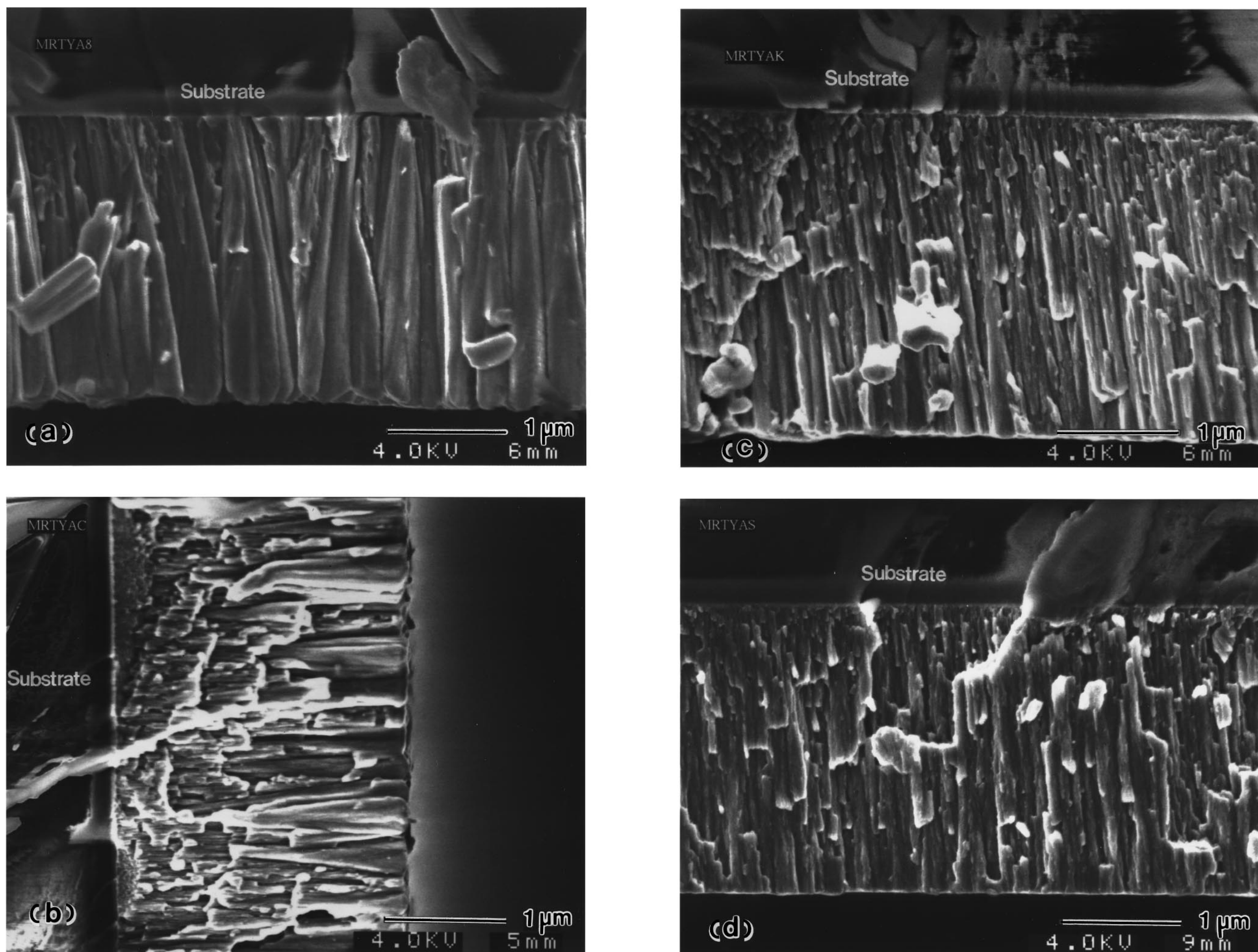

FIG. 7. (a)–(d) SEM cross-sectional micrographs of films deposited in (a) 0%, (b) 2%, (c) 6%, and (d) 10% N_2.

Fig. 6(b). It shows the ⟨111⟩ zone axis of the sendust. It appears to contain two adjacent sets of diffraction spots which suggest the possible existence of two slightly misoriented subgrains. A ring SAD pattern was found, as shown in Fig. 6(c), from an area labeled B in Fig. 4(b), which contains several small 20 nm grains. This indicates that the small grains are nearly randomly oriented. In the film deposited in 6% N_2, the small grains are shown to occupy an even larger percentage of the area as seen in Fig. 4(c). The larger grains appear to have a slightly reduced size of about 140 nm. The TEM micrograph of the film deposited in 10% N_2 as seen in Fig. 4(d) shows only small grains. Some of these small grains seem to form clusters of about 100 nm which are similar to the larger grains in the films with lower N_2 content. The film without N_2 seems to be more porous than the films containing N_2. The higher porosity in the film without N_2 as suggested by the TEM studies is consistent with its lower value of M_s.

SEM cross-sectional views of fractured films with different N_2 contents (0%, 2%, 6%, and 10% N_2 in the sputtering gas) are shown in Fig. 7. Columnar film structures were observed in all films studied. Distinctive power-law cone structures[12] were observed in the film without N_2 to extend through the film thickness; whereas, in the film deposited in 2% N_2, while some long cones are present, they are mixed with much narrower needlelike structures, especially near the substrate surface. In the films deposited in 6% and 10% N_2, only needlelike structures are present. These needlelike columns have an average diameter of roughly 150 nm; whereas, the cone structures have an average diameter of about 200–250 nm. It is believed that the growth of power-law cones in the film without N_2 may yield voids or noncrystalline regions in between them, which result in less dense microstructures. The size of the large grains in the film without N_2 and of clusters of the smaller grain in the N_2 containing films measured from the TEM micrographs is in agreement with the diameters of the conelike or needlelike cross-sectional morphological features measured from the SEM micrographs. Although columnar cross-sectional morphological structures were observed in these films, it is unlikely that grains as small as 20 nm could have columnar growth and extend through the 3 μm film thickness.

The surface roughness of the films (R_a) measured using both AFM and ellipsometry are shown in Fig. 8. R_a was found to decrease monotonically with increasing N_2 content.

The electrical resistivity of the films deposited in 10% N_2 gas was 30% higher than that of the film without N_2 as

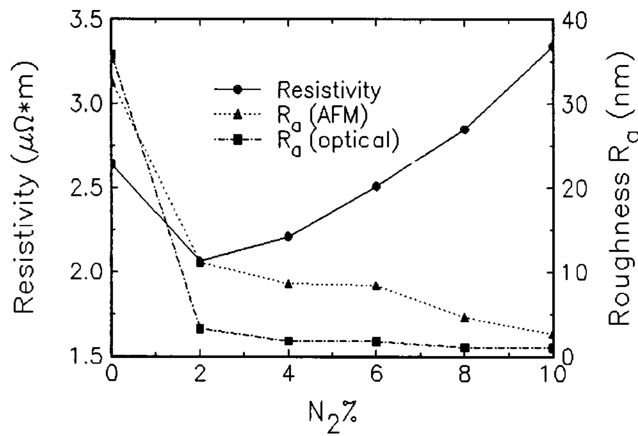

FIG. 8. The resistivity and the surface roughness measured using both AFM and ellipsometry.

also seen in Fig. 8. An initial drop in the resistivity was observed when 2% N_2 was introduced. The resistivity then gradually increased as more N_2 was added. The high resistivity in the film without N_2 is likely due to its high porosity. The increase in the electrical resistivity and the reduction in the surface roughness as N_2% was increased from 2% to 10% in the gas are consistent with the reduction in the grain size of the films. These values of resistivity are one or two orders of magnitude higher than in most metals. High electrical resistivity is one of the desirable characteristics of sendust for many applications in magnetic recording technology.

As shown in Fig. 9, the refraction index n, the extinction coefficient k, and the reflectance of the surface R were all observed to experience an increase and then a gradual decrease with the increase of N_2% in the sputtering gas. The low values of the optical constants n and k, and the reflectance R of the film without N_2 are also due to the high porosity and large surface roughness of the film, which makes it less refractive, absorptive, and reflective. The change in n, k, and R were slight in the films deposited from 2% to 10% N_2.

XPS analysis were performed on sendust films with 0%, 2%, 6%, and 10% N_2 in the sputtering gas. The depth profiles revealed that the films contain oxygen and carbon in the top 5 nm of the films due to the surface contamination. The atomic concentrations of each element in the films were measured at a depth of 10 nm, and are shown in Table III.

TABLE III. Atomic concentration of elements.

N_2%	Fe (at %)	Al (at %)	Si (at %)	N (at %)
0%	81	7	8	0
2%	78	8	9	3
6%	74	8	8	8
10%	68	8	8	10

The binding energy spectra of N $(1s)$ of the N_2 containing films showed a single peak at 397 eV, corresponding to a negative energy shift of 3 eV from the molecular nitrogen state.[13] They showed double peaks at the depth of <2 nm, possibly due to surface contamination by some organic substances.

In all films studied, the Fe $(2p_{3/2})$ spectra show no observable energy shift from their pure metallic iron state. The double peaks observed at the depth of <2 nm are believed to be due to surface oxidization.

The binding energy spectra of Al $(2s)$ exhibited an interesting change as the N_2% increased in the sputtering gas as shown in Fig. 10. In the film deposited without N_2, the binding energy of Al $(2s)$ at a depth of 12 nm exhibits only a single peak at 117.6 eV, which corresponds to the metallic Al state;[13] whereas, in the film deposited in 10% N_2, there is a single peak at 119.4 eV at the same depth, which may be due to the formation of AlN. This energy shift was not believed to be due to Al_2O_3 since the oxygen concentration at that depth is much lower than N_2 and lacks the systematic patterns of change with N_2%. In the samples deposited with

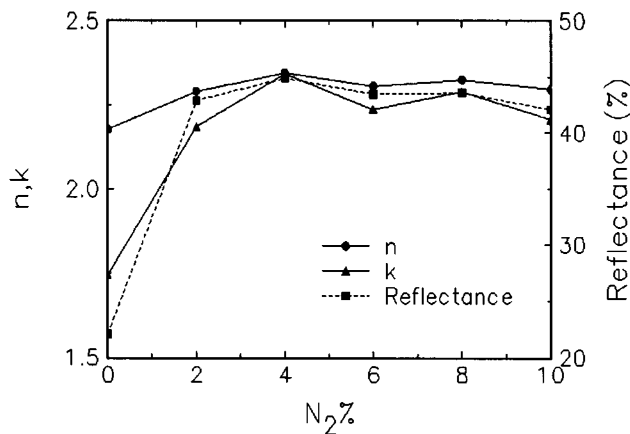

FIG. 9. The index of refraction n, the extinction coefficient k, and the reflectance measured using ellipsometry.

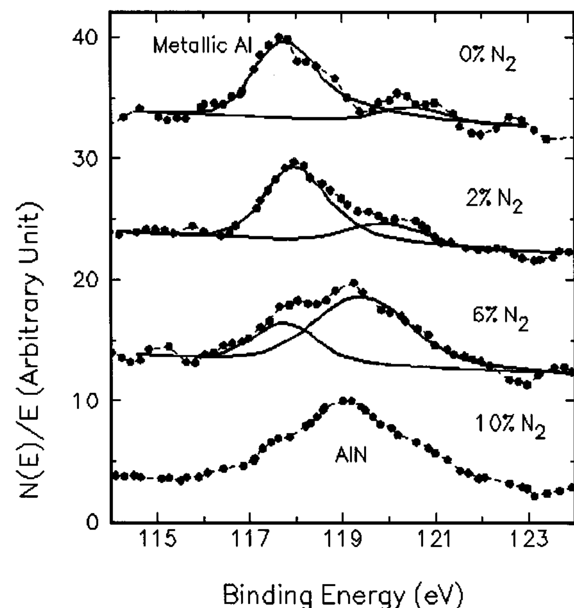

FIG. 10. Binding energy spectra of Al $(2s)$ at depth of 12 nm in films deposited in 0%, 2%, 6%, and 10% N_2, respectively. The solid circles represent the experimental data points. The solid lines are peak fit results.

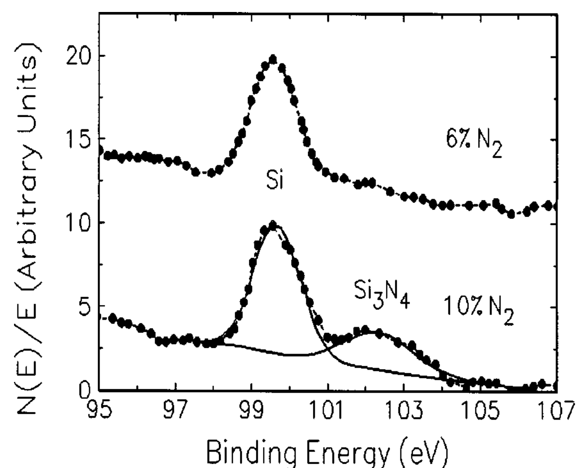

FIG. 11. Binding energy spectra of Si $(2p)$ at depth of 12 nm for films deposited in 6% and 10% N_2 The solid circles are experimental data points. The solid lines represent peak fit results.

an intermediate percentage of N_2 gas, namely 2% and 6%, the partitioning of the peaks area into the lower and the higher energy peaks, which corresponds to metallic Al, and in AlN are 22.9%/77.1%, and 72.7%/27.3%, respectively.

The spectra of Si $(2p)$ exhibit a single peak at 99.6 eV in the films deposited in 0%, 2%, and 6% N_2 at the depth of 12 nm. This peak corresponds to elemental Si. The peak which indicates the existence of Si_3N_4 (101.8 eV),[13] was not observed even in the film deposited in 6% N_2 as shown in Fig. 11. The spectrum of Si $(2p)$ at the depth of 12 nm in the film deposited in 10% N_2 is also shown in Fig. 11 and exhibits a second peak at an energy of 101.9 eV, which is very close to that due to the formation of Si_3N_4. The ratio of the peak areas in the higher and lower energy peaks is 34.5%/ 65.6%.

IV. DISCUSSION AND CONCLUSION

Yang *et al.* simulated the cross-sectional morphology of thin films with columnar microstructure by considering nucleation and growth of power-law cones.[14] The results showed that when nucleation only occurs at the substrate surface, the power-law cone structures were shown to extend through the film thickness, and the nodular growth greatly roughens the surface. When nucleation occurs throughout the film thickness due to a greater number of nucleation sites, needlelike morphological features result. Our cross-sectional SEM studies of sendust films without and with N_2 seem to agree with these simulation results. The change in the surface roughness as indicated both by AFM and ellipsometry measurements are correlated with the morphological change in the films, which is consistent with the simulation results.[14]

XPS binding energy spectra of the elements suggest that N_2 in the films reacts with Al preferentially to form AlN. Si_3N_4 may be formed in the film deposited in 10% N_2, in which the atomic concentration of nitrogen becomes higher than that of Al as shown in Table III. Iron is probably present in the metallic chemical state in the bulk.

It is believed that the precipitation of AlN at the grain boundaries may become nucleation centers and greatly enhance the nucleation rate. It may also have inhibited the grain growth of α-Fe, Smaller grain size and softer magnetic properties are therefore achieved. Forming Si_3N_4, however, may have deteriorated the magnetic properties of the films. The optimum nucleation density may be obtained without disrupting the soft magnetic properties when the atomic concentrations of Al and N become equal.

Herzer[15] used the random anisotropy model originally proposed by Alben *et al.*[16] to interpret the grain size dependence of coercivity in soft magnetic materials. He proposed that, when the grain size is below the ferromagnetic exchange length L_{ex}, the effective anisotropy in an assembly of grains is determined not by the anisotropy of each individual grain as for large grains, but by an average over several grains due to the ferromagnetic exchange interaction. In fact, according to this model, the coercivity is strongly dependent on the grain size D and varies as D^6, while the permeability varies as $1/D^6$. If the grain size is larger than the domain wall width, on the other hand, the magnetization process is determined by domain wall pinning with the coercivity varies as $1/D$. For the amorphous α-FeSi ribbon used in his study, the values of exchange length and domain wall width were estimated to be 35 and 150 nm, respectively.

Hoffmann *et al.*[17] calculated the wall coercive force by considering the local fluctuation of the wall energy, which was determined by the average of the local anisotropy of the crystallites included in the wall volume. In a polycrystalline film in which the size of crystallites D does not grow with film thickness, he found that the wall coercivity $H_w \propto D^2$.

The reduction in H_c and improvement in permeabilities, which were accompanied by the reductions in grain size in the sendust films we studied, can be qualitatively explained by both models. The increase of N_2 from 0% to 6% in the gas dramatically reduced the average grain size from 200 to about 20 nm. These grains of 20 nm average size were found to be randomly oriented as also suggested by the TEM microdiffraction patterns. It is believed that the grain size of 20 nm in the N_2 containing films is below the exchange length so that the reduction in coercivity with grain size is observed. The grain size of 200 nm in the film without N_2 may be within the range where coercivity is relatively insensitive to the grain size. The value of coercivity was observed to decrease by a factor of about 66 as the N_2 content increased, while the grain size was reduced by a factor of 10. Our data are insufficient to suggest which theoretical model provides a better fit to the experimental results. The film deposited with 10% N_2 showed fine uniform grain features; however, the selective nitriding of Si atoms was also found, which may have led to the observed degradation of the magnetic properties. The degradation of the magnetic properties due to the selective nitriding of Si may be related to the change in magnetostriction and film stress.

ACKNOWLEDGMENTS

The authors would like to thank and acknowledge works by colleagues at Seagate, Dr. Darrell R. Louder for AFM measurements; Trent J. Mckay and Dr. Songsheng Xue for help on sputter deposition; Declan Macken for sample an-

nealing; H. Erskine for providing SEM micrographs, and A. Rodnyansky of Katz Analytical Services for XPS data and Dr. Robert C. Jones of Carnegie Mellon University for helpful discussions.

[1] M. I. Ullah, K. R. Coffey, M. A. Parker, and J. K. Howard, IEEE Trans. Magn. **30**, 3927 (1994).
[2] T. M. Coughlin, IEEE Trans. Magn. **21**, 1897 (1985).
[3] M. Miura, K. Tanaka, and Y. Noro, J. Appl. Phys. **25**, 1192 (1986).
[4] M. Miyazaki, M. Ichikawa, T. Komatsu, K. Matusita, and K. Nakajima, J. Appl. Phys. **69**, 1556 (1991).
[5] T. Wakiyama, M. Takahashi, S. Nishimaki, and J. Shimoda, IEEE Trans. Magn. **MAG-17**, 3147 (1981).
[6] M. Takahashi, H. Arai, T. Tanaka, and T. Wakiyama, IEEE Trans. Magn. **22**, 638 (1990).
[7] M. Takahashi and T. Shimatsu, IEEE Trans. Magn. **26**, 1485 (1990).
[8] T. Kumura, K. Yamauchi, and T. Kobayashi, J. Appl. Phys. **61**, 3844 (1987).
[9] N. Hayashi, S. Yoshimura, and J. Numazawa, NHK Laboratories Note, 377, 1990 (unpublished).
[10] S. Chikazumi and S. H. Charap, *Physics of Magnetism* (Krieger, New York, 1964).
[11] L. L. Kazmerski, *Advanced Materials and Device Analytical Techniques* (Plenum, New York, 1986).
[12] R. Messier and J. E. Yehoda, J. Appl. Phys. **58**, 3739 (1985).
[13] J. F. Moulder, W. F. Stickle, P. E. Sobol, and K. D. Bomben, *Handbook of X-ray Photoelectron Spectroscopy* (Perkin Elmer, Eden Prairie, MN, 1992).
[14] B. Yang, B. L. Walden, R. Messier, and W. B. White, Proc. SPIE **821**, 68 (1987).
[15] G. Herzer, IEEE Trans. Magn. **26**, 1397 (1990).
[16] R. Alben, J. J. Becker, and M. C. Chi, J. Appl. Phys. **49**, 1653 (1978).
[17] H. Hoffmann and T. Fujii, J. Magn. Magn. Mater. **128**, 395 (1993).